Journal of Computational Physics 352 (2018) 172–189

Contents lists available at ScienceDirect

Journal of Computational Physics

www.elsevier.com/locate/jcp

Semi-analytical Karhunen–Loeve representation of irregular waves based on the prolate spheroidal wave functions

Gibbeum Lee, Yeunwoo Cho *

Department of Mechanical Engineering, Korea Advanced Institute of Science and Technology, 291 Daehak-ro, Yuseong-gu, Daejeon, 34141, Republic of Korea

ARTICLE INFO

Article history:
Received 2 June 2017
Received in revised form 4 September 2017
Accepted 13 September 2017
Available online 28 September 2017

Keywords:
Karhunen–Loeve expansion
Prolate spheroidal wave function

ABSTRACT

A new semi-analytical approach is presented to solving the matrix eigenvalue problem or the integral equation in Karhunen–Loeve (K–L) representation of random data such as irregular ocean waves. Instead of direct numerical approach to this matrix eigenvalue problem, which may suffer from the computational inaccuracy for big data, a pair of integral and differential equations are considered, which are related to the so-called prolate spheroidal wave functions (PSWF). First, the PSWF is expressed as a summation of a small number of the analytical Legendre functions. After substituting them into the PSWF differential equation, a much smaller size matrix eigenvalue problem is obtained than the direct numerical K–L matrix eigenvalue problem. By solving this with a minimal numerical effort, the PSWF and the associated eigenvalue of the PSWF differential equation are obtained. Then, the eigenvalue of the PSWF integral equation is analytically expressed by the functional values of the PSWF and the eigenvalues obtained in the PSWF differential equation. Finally, the analytically expressed PSWFs and the eigenvalues in the PWSF integral equation are used to form the kernel matrix in the K–L integral equation for the representation of exemplary wave data such as ordinary irregular waves. It is found that, with the same accuracy, the required memory size of the present method is smaller than that of the direct numerical K–L representation and the computation time of the present method is shorter than that of the semi-analytical method based on the sinusoidal functions.

© 2017 Elsevier Inc. All rights reserved.

1. Introduction

Karhunen–Loeve (K–L) representation of random or irregular data is the optimal representation which minimizes the root-mean-squared error between the original data $\zeta(t)$ and the truncated version of the original data $\zeta_N(t)$, where t is time and N is the number of data points. In the area of fluid mechanics, K–L representation was frequently used in the area of turbulent flow analysis [1–5]. In K–L representation, the bases are obtained from the data themselves to be analyzed, i.e., adaptive. As a result, the shapes of the bases closely resemble the target data. On the contrary, other kinds of representation use fixed bases independent of data to be analyzed. One such example is the conventional Fourier representation whose bases are sinusoidal functions. For the same small number of each own bases, the K–L representation using data-dependent

* Corresponding author.
E-mail address: ywoocho@kaist.ac.kr (Y. Cho).

https://doi.org/10.1016/j.jcp.2017.09.023
0021-9991/© 2017 Elsevier Inc. All rights reserved.

Nomenclature

t	Time	η, ξ, θ	Prolate spheroidal coordinates
$\zeta(t)$	Continuous wave elevation data	$K(t-t')$	Autocorrelation of the N-point data $\zeta_N(t)$ to be analyzed
$\zeta_N(t)$	N-point discrete wave elevation data	$\phi_j(t)$	Eigenvectors in the Karhunen–Loeve expansion
T	Half of the temporal range of the data	κ_j	Eigenvalues in the Karhunen–Loeve expansion
ω	Wave angular frequency	$P_n(\eta)$	The Legendre function ($n = 0, 1, 2, \ldots$)
Ω	Maximum frequency in the data	$S_n(c, \eta)$	The prolate spheroidal wave function ($n = 0, 1, 2, \ldots$)
$P(\omega)$	Power spectral density function	$\chi_n(c)$	Eigenvalues of the PSWF differential equation
ω'	Dimensionless wave angular frequency, ω/Ω	$\lambda_n(c)$	Eigenvalues of the PSWF integral equation
τ'	Dimensionless time, t/T		
$c = \Omega T$	Dimensionless bandwidth		

adaptive bases is usually better than conventional Fourier representation using data-independent fixed bases. In other words, the K–L representation features faster convergence than other kinds such as Fourier. For the K–L representation, however, one needs to numerically solve the following integral-equation type eigenvalue problem whose kernel $K(t-t')$ is the autocorrelation of the N-point data $\zeta_N(t)$ to be analyzed.

$$\int_{-T}^{T} K(t-t')\phi_j(t')dt' = \kappa_j \phi_j(t), \tag{1}$$

where $[-T, T]$ (s) is the time interval of wave-elevation data $\zeta_N(t)$. By solving this equation, one obtains a set of eigenvectors $\phi_j(t)$ (along with the eigenvalues κ_j) which play roles as orthonormal bases in the K–L representation.

$$\zeta_N(t) = \sum_{j=0}^{N-1} a_j \phi_j(t); \qquad a_j = \int_{-T}^{T} \zeta_N(t)\phi_j(t)dt \tag{2}$$

The relevant matrix size is N by N in the numerical eigenvalue problem. Therefore, for big data, such as ocean irregular wave data, the matrix size may become too big for the computation result to be reliable [6]. Therefore, instead of direct numerical calculation of Eq. (1), we suggest a new semi-analytical procedure to be introduced in the computation such that a more reliable result can be obtained with smaller matrix eigenvalue problems.

Our present interest is in the K–L representation of irregular wave-elevation data $\zeta_N(t)$ during a certain time interval $[-T, T]$ (s). The data are assumed to be stationary random process. From the data, the power spectrum density function $P(\omega)$ (ω: rad/s) can easily be computed thanks to the development of FFT (Fast Fourier Transform). Typical examples of the ocean power spectra are JONSWAP [7] and Pierson–Moskowitz spectra [8]. Usually, the spectrum is band-limited, $[-\Omega, \Omega]$ (rad/s). Then, the Wiener–Khinchin theorem states that the kernel of the relevant integral equation or the autocorrelation of the data is the inverse Fourier transform of the power spectrum density function.

$$K(t-t') = \frac{1}{2T}\int_{-T}^{T} \zeta(t)\zeta(t')dt = \frac{1}{2\pi}\int_{-\Omega}^{\Omega} P(\omega)\exp(-i\omega t')\exp(i\omega t)d\omega \tag{3}$$

Rather than calculating the above integral directly, the exponential term $\exp(i\omega t)$ can be expressed using Mercer's theorem [9] such that

$$\exp(i\omega t) = \exp\left(i\frac{\omega}{\Omega}\frac{t}{T}\Omega T\right) = \exp(i\omega'\tau' c) = \sum_{j=0}^{\infty} \lambda_j(c) S_j(c, \omega') S_j(c, \tau'), \tag{4}$$

where $\omega/\Omega = \omega'$, $t/T = \tau'$, $\Omega T = c$, the function $S_j(c, \tau')$ is the eigenvector and $\lambda_j(c)$ is the eigenvalue of the following integral-equation type eigenvalue problem.

$$\int_{-1}^{1} \exp(ic\omega'\tau') S_j(c, \omega')d\omega' = \lambda_j(c) S_j(c, \tau') \tag{5}$$

The function $S_j(c, \tau')$ is called as the prolate spheroidal wave function (PSWF) [10–13]. To find PSWFs, this equation can be numerically solved directly as done in [14]. The matrix size involved is N by N, which may become also prohibitively large for big data as already mentioned.

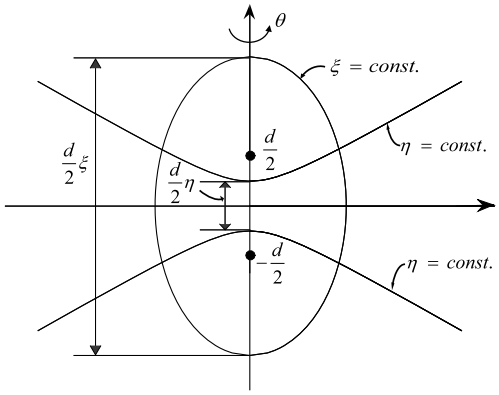

Fig. 1. Prolate spheroidal coordinate (ξ, η, θ). A constant-ξ curve is an ellipse and a constant-η curve is a hyperbola whose foci are located on the z-axis. When rotated 2π about the z-axis, these curves become a prolate spheroid and a hyperboloid, respectively.

To date, two kinds of numerical methods have been developed for the K–L representation of random data in the area of fluid mechanics. The first one is the direct numerical solution of Eqs. (1) and (2) [1–5], and the second one is the indirect numerical solution based on Eqs. (1)–(5) using PSWFs [14]. As mentioned above, however, these kinds of direct numerical approach may suffer from the computational inaccuracy as the data size increases. Therefore, to minimize the numerical work involved, we suggest a semi-analytical method for the K–L representation based on Eqs. (1)–(5). The key idea is to use the PSWF differential equation corresponding to PSWF integral equation Eq. (5). First, we assume that the PSWF is a summation of a small number of the Legendre functions. The analytical expressions of the Legendre functions and its derivatives are well known. After substituting them into the PSWF differential equation (to be explained in section 2), we will obtain a much smaller size matrix eigenvalue problem than the direct K–L matrix eigenvalue problem. By solving this with a minimal numerical effort, the PSWF (eigenvector) $S_j(c, \tau')$ and the associated eigenvalue $\chi_j(c)$ of the PSWF differential equation will be obtained. Then, the eigenvalue $\lambda_j(c)$ of the PSWF integral equation Eq. (5) will be analytically obtained from the value of the parameter c, the central values of the PSWF (or its derivatives) and the eigenvalues $\lambda_j(c)$ obtained in the PSWF differential equation. In a general sense, the present method can be categorized as a Galerkin method using the PSWF compared to other kinds of Galerkin methods using sinusoidal functions [15,16] or wavelets [17].

With this overview in mind, in section 2, the PSWF differential equation will be derived, which originates from the Helmholtz equation in the prolate spheroidal coordinate. In section 3, the relationship between the PSWF differential- and integral equations will be described. In section 4, solution procedure of PSWF differential- and integral equations will be explained. In section 5, this newly suggested semi-analytical K–L representation will be applied to the analysis of an exemplary wave data with comparison to results from the conventional purely numerical K–L expansion and a semi-analytical method using sinusoidal functions. Finally, section 6 is the concluding remark.

2. PSWF differential equation

In Cartesian coordinate, the general 3-D wave equation reads

$$\frac{\partial^2 u}{\partial t^2} = c_0^2 \nabla^2 u, \tag{6}$$

where c_0 is the wave propagation speed. By assuming $u = F(x, y, z)\exp(i\omega t)$, Eq. (6) becomes following Helmholtz equation.

$$\left(\nabla^2 + k^2\right)F = 0; \quad k = \omega/c_0, \tag{7}$$

where $\nabla^2 = \partial^2/\partial x^2 + \partial^2/\partial y^2 + \partial^2/\partial z^2$ is the Laplacian operator, k is the wavenumber. Instead of Cartesian coordinate, one may solve Eq. (7) in the prolate spheroidal coordinate whose name originates from the spheroid obtained by rotating an ellipse whose foci are $f_1(0, 0, d/2)$ and $f_2(0, 0, -d/2)$ in the (x, z) plane or (y, z) plane about z axis with the angular amount $\theta = 2\pi$, to which longer major axis of the ellipse is parallel as shown in Fig. 1. Between the prolate spheroidal coordinate (η, ξ, θ) and Cartesian coordinate (x, y, z), following relationship holds.

$$x = \frac{1}{2}d\sqrt{\left(\xi^2 - 1\right)\left(1 - \eta^2\right)}\cos\theta \tag{8}$$

$$y = \frac{1}{2}d\sqrt{\left(\xi^2 - 1\right)\left(1 - \eta^2\right)}\sin\theta \tag{9}$$

$$z = \frac{\xi\eta d}{2} \tag{10}$$

Now, from Eqs. (7)–(10), the Helmholz equation in the prolate spheroidal coordinate turns out to be

$$\left\{\frac{d}{d\eta}\left((1-\eta^2)\frac{d}{d\eta}\right)+\frac{d}{d\xi}\left((\xi^2-1)\frac{d}{d\zeta}\right)+\frac{\xi^2-\eta^2}{(\xi^2-1)(1-\eta^2)}\frac{d^2}{d\theta^2}+c^2(\xi^2-\eta^2)\right\}F=0;\quad c=\frac{1}{2}kd \tag{11}$$

Using the method of separation of variables, let us assume that $F=F(\eta,\xi,\theta)$ has the following form.

$$F(\eta,\xi,\theta)=S(c,\eta)R(c,\xi)\Theta(\theta) \tag{12}$$

By substituting Eq. (12) into Eq. (11),

$$\frac{1}{S}\frac{d}{d\eta}\left\{(1-\eta^2)\frac{dS}{d\eta}\right\}-c^2\eta^2+\frac{1}{R}\frac{d}{d\xi}\left\{(\xi^2-1)\frac{dR}{d\xi}\right\}+c^2\xi^2+\left(\frac{1}{1-\eta^2}+\frac{1}{\xi^2-1}\right)\frac{1}{\Theta}\frac{d^2\Theta}{d\theta^2}=0 \tag{13}$$

Let us define the separation constant m^2 for $\Theta(\theta)$ as follows.

$$\frac{1}{\Theta}\frac{d^2\Theta}{d\theta^2}=-m^2 \tag{14}$$

Then, both S and R depend upon m. Thus, by replacing S and R with S_m and R_m,

$$\frac{1}{S_m}\frac{d}{d\eta}\left\{(1-\eta^2)\frac{dS_m}{d\eta}\right\}-c^2\eta^2-\frac{m^2}{1-\eta^2}+\frac{1}{R_m}\frac{d}{d\xi}\left\{(\xi^2-1)\frac{dR_m}{d\xi}\right\}+c^2\xi^2-\frac{m^2}{\xi^2-1}=0 \tag{15}$$

Now, let us define the separation constant $\chi_m(c)$ as follows.

$$\frac{1}{S_m}\frac{d}{d\eta}\left\{(1-\eta^2)\frac{dS_m}{d\eta}\right\}-c^2\eta^2-\frac{m^2}{1-\eta^2}=-\chi_m(c) \tag{16}$$

$$\frac{1}{R_m}\frac{d}{d\xi}\left\{(\xi^2-1)\frac{dR_m}{d\xi}\right\}+c^2\xi^2-\frac{m^2}{\xi^2-1}=\chi_m(c) \tag{17}$$

Eq. (16) and Eq. (17) are essentially eigenvalue problems, where whose nth eigenvalue and eigenvector solutions are denoted by χ_{mn}, S_{mn}, R_{mn}, respectively. In particular, the eigenvector solutions to Eq. (16) for $m=0$ are called as prolate spheroidal wave functions (PSWF). Hereafter, the eigenvalue $\chi_{0n}(c)$ will be denoted by $\chi_n(c)$, the corresponding eigenvector, i.e., the PSWF, $S_{0n}(c,\eta)$ will be denoted by $S_n(c,\eta)$, and Eq. (16) for $m=0$ will be called as the PSWF differential equation.

3. Derivation of the PSWF integral equation from the PSWF differential equation

From the previous section, the PSWF differential equation reads

$$D_\eta S_n(c,\eta)+\chi_n(c)S_n(c,\eta)=0;\quad |\eta|\le 1, \tag{18}$$

where

$$D_\eta=\frac{d}{d\eta}\left\{(1-\eta^2)\frac{d}{d\eta}\right\}-c^2\eta^2. \tag{19}$$

Then, consider the following Sturm–Liouville type integral about PSWF, $S_n(c,\eta)$ and an arbitrary function $Q(c,\eta,\xi)$.

$$\int_{-1}^{1}(S_nD_\eta Q-QD_\eta S_n)d\eta \tag{20}$$

By direct substitution of Eq. (19) into Eq. (20) and integration by parts, one may easily verify that Eq. (20) is always equal to zero as follows.

$$\begin{aligned}
&\int_{-1}^{1}(S_nD_\eta Q-QD_\eta S_n)d\eta\\
&=\int_{-1}^{1}S_n\left(\frac{d}{d\eta}\left\{(1-\eta^2)\frac{dQ}{d\eta}\right\}-c^2\eta^2Q\right)-Q\left(\frac{d}{d\eta}\left\{(1-\eta^2)\frac{dS_n}{d\eta}\right\}-c^2\eta^2S_n\right)d\eta\\
&=\int_{-1}^{1}S_n\frac{d}{d\eta}\left\{(1-\eta^2)\frac{dQ}{d\eta}\right\}-Q\frac{d}{d\eta}\left\{(1-\eta^2)\frac{dS_n}{d\eta}\right\}d\eta\\
&=S_n\frac{d}{d\eta}\left\{(1-\eta^2)\frac{dQ}{d\eta}\right\}\Big|_{-1}^{1}-\int_{-1}^{1}\frac{dS_n}{d\eta}\left\{(1-\eta^2)\frac{dQ}{d\eta}\right\}d\eta-Q\frac{d}{d\eta}\left\{(1-\eta^2)\frac{dS_n}{d\eta}\right\}\Big|_{-1}^{1}+\int_{-1}^{1}\frac{dQ}{d\eta}\left\{(1-\eta^2)\frac{dS_n}{d\eta}\right\}d\eta\\
&=0
\end{aligned} \tag{21}$$

In other words, following self-adjoint relation holds.

$$\int_{-1}^{1} S_n D_\eta Q\, d\eta = \int_{-1}^{1} Q\, D_\eta S_n d\eta \tag{22}$$

Then, let us think of the following differential equation with respect to η and ζ.

$$(D_\eta - D_\zeta) Q(c, \eta, \zeta) = 0, \tag{23}$$

whose solution is

$$Q(c, \eta, \zeta) = \exp(ic\eta\zeta) \tag{24}$$

Then, from Eq. (23), the LHS of Eq. (22) is

$$\int_{-1}^{1} S_n D_\eta Q\, d\eta = \int_{-1}^{1} S_n(c, \eta) D_\zeta Q\, d\eta = D_\zeta \int_{-1}^{1} S_n Q\, d\eta \tag{25}$$

The RHS of Eq. (22) is, from Eq. (18),

$$\int_{-1}^{1} Q\, D_\eta S_n d\eta = -\chi_n(c) \int_{-1}^{1} Q\, S_n d\eta \tag{26}$$

Therefore, from Eq. (25) and Eq. (26),

$$\big(D_\zeta + \chi_n(c)\big) \int_{-1}^{1} Q\, S_n d\eta = 0 \tag{27}$$

By comparison of Eq. (27) with Eq. (18), $(D_\zeta + \chi_n(c)) S_n = 0$, one can conclude that

$$\int_{-1}^{1} Q\, S_n d\eta = \lambda_n(c) S_n, \tag{28}$$

where $\lambda_n(c)$ is a constant. Then, from Eq. (24),

$$\int_{-1}^{1} S_n \exp(ic\eta\zeta) d\eta = \lambda_n(c) S_n. \tag{29}$$

This is the PSWF integral equation derived from the PSWF differential equation, which is essentially also an eigenvalue problem, whose eigenvector is the same PSWF as that of the PSWF differential equation and the corresponding eigenvalue is $\lambda_n(c)$. In the next section, the PSWF, $S_n(c, \eta)$ and the value of $\chi_n(c)$ will be obtained almost analytically based on the PSWF differential equation Eq. (18). Then, these are used to find the eigenvalue $\lambda_n(c)$ of the PSWF integral equation Eq. (29).

4. Solutions of PSWF differential- and integral equations

4.1. Eigenvalues and eigenvectors of PSWF differential equation

The PSWF differential equation for a nonzero c is

$$\frac{d}{d\eta}\left\{(1-\eta^2)\frac{dS_n(c,\eta)}{d\eta}\right\} + \big(\chi_n(c) - c^2\eta^2\big) S_n(c, \eta) = 0. \tag{30}$$

When $c = 0$, by letting $\chi_n(c = 0) = n(n+1)$, Eq. (30) becomes the well-known Legendre equation whose solution is the Legendre function $P_n(\eta)$, i.e., $P_n(\eta) = S_n(c = 0, \eta)$ for $-1 \le \eta \le 1$.

$$\frac{d}{d\eta}\left\{(1-\eta^2)\frac{dP_n(\eta)}{d\eta}\right\} + n(n+1) P_n(\eta) = 0 \tag{31}$$

Now, for $c \neq 0$, let us assume that the PSWF $S_n(c, \eta)$ can be represented by the superposition of the Legendre functions as follows.

$$S_n(c,\eta)=\sum_{r=0}^{\infty} d_{2r+s}^n(c)P_{2r+s}(\eta)\approx\sum_{r=0}^{M-1} d_{2r+s}^n(c)P_{2r+s}(\eta);\quad s=\begin{cases}0 & (n=0,2,4,\ldots)\\ 1 & (n=1,3,5,\ldots),\end{cases} \tag{32}$$

where the coefficient $d_{2r+s}^n(c)$ is yet unknown. By substituting Eq. (32) into Eq. (30), one obtains the following eigenvalue problem.

$$A_{2r+s}d_{2r-2+s}^n+B_{2r+s}d_{2r+s}^n+C_{2r+s}d_{2r+2+s}^n=\chi_n(c)d_{2r+s}^n;\quad r=0,1,2,\ldots,M-1, \tag{33}$$

where

$$A_{2r+s}(c)=c^2\frac{(2r+s)(2r+s-1)}{(4r+2s-1)(4r+2s-3)}, \tag{34}$$

$$B_{2r+s}(c)=(2r+s)(2r+s+1)+c^2\frac{2(2r+s)(2r+s+1)-1}{(4r+2s-1)(4r+2s+3)}, \tag{35}$$

$$C_{2r+s}(c)=c^2\frac{(2r+s+1)(2r+s+2)}{(4r+2s+3)(4r+2s+5)}. \tag{36}$$

In more detail, Eq. (33) reads as follows.

$$\begin{aligned}
&r=0: A_s d_{-2+s}^n+B_s d_s^n+C_s d_{2+s}^n=\chi_n(c)d_s^n\\
&r=1: A_{2+s}d_s^n+B_{2+s}d_{2+s}^n+C_{2+s}d_{4+s}^n=\chi_n(c)d_{2+s}^n\\
&\cdots\\
&r=M-2: A_{2M-4+s}d_{2M-6+s}^n+B_{2M-4+s}d_{2M-4+s}^n+C_{2M-4+s}d_{2M-2+s}^n=\chi_n(c)d_{2M-4+s}^n\\
&r=M-1: A_{2M-2+s}d_{2M-4+s}^n+B_{2M-2+s}d_{2M-2+s}^n+C_{2M-2+s}d_{2M+s}^n=\chi_n(c)d_{2M-2+s}^n
\end{aligned} \tag{37}$$

In the above equation, there are $M+2$ unknowns $[d_{-2+s}^n, d_s^n, d_{2+s}^n,\ldots,d_{2M-4+s}^n, d_{2M-2+s}^n, d_{2M+s}^n]$ in the LHS while M unknowns $[d_s^n, d_{2+s}^n,\ldots,d_{2M-4+s}^n, d_{2M-2+s}^n]$ in the RHS. This dimensional inconsistency originates from the finite-sum approximation of the infinite sum in Eq. (32). First, in Eq. (37), the coefficient $A_s(c)$ is zero for $r=0$ since

$$A_s(c)=c^2\frac{s(s-1)}{(2s-1)(2s-3)}=0\quad\text{for } s=0,1 \tag{38}$$

Therefore, we set $d_{-2+s}^n=0$. We also assume $d_{2M+s}^n=0$ by setting $C_{2M-2+s}=0$, which will be analytically true for the original infinite tridiagonal matrix [18]. This will be justified if resultant M unknown coefficients $[d_s^n, d_{2+s}^n,\ldots,d_{2M-4+s}^n, d_{2M-2+s}^n]$ turn out to be in the form of $[d_s^n, d_{2+s}^n,\ldots,0,0,\ldots,0,0]$. If $d_{2M-2+s}^n\neq 0$, the corresponding coefficient vector is neglected in Eq. (32). By trial and error, the borderline "n" turns out to be $[2c/\pi+\log_{10}c]$ (Gauss' symbol). This value is also the borderline "n" between nonzero eigenvalues and zero eigenvalues of a certain size of matrix eigenvalue problem, Eq. (29) [13]. Now, Eq. (33) can be rewritten as a following tridiagonal-matrix eigenvalue equation whose size is M by M (even and odd modes each), where M can be much smaller than the number of original data points N.

$$\begin{bmatrix}
B_s & C_s & 0 & 0 & \cdots & \cdots & \cdots & 0\\
A_{2+s} & B_{2+s} & C_{2+s} & 0 & \ddots & \ddots & \ddots & \vdots\\
0 & A_{4+s} & B_{4+s} & C_{4+s} & \ddots & \ddots & \ddots & \vdots\\
0 & 0 & \ddots & \ddots & \ddots & \ddots & \ddots & \vdots\\
\vdots & \ddots & \ddots & A_{2r-2+s} & B_{2r-2+s} & C_{2r-2+s} & 0 & 0\\
\vdots & \ddots & \ddots & \ddots & \ddots & \ddots & \ddots & 0\\
\vdots & \ddots & \ddots & \ddots & 0 & A_{2M-4+s} & B_{2M-4+s} & C_{2M-4+s}\\
0 & \cdots & \cdots & \cdots & 0 & 0 & A_{2M-2+s} & B_{2M-2+s}
\end{bmatrix}
\begin{bmatrix} d_s^n\\ d_{2+s}^n\\ d_{4+s}^n\\ \vdots\\ d_{2r-2+s}^n\\ \vdots\\ d_{2M-4+s}^n\\ d_{2M-2+s}^n \end{bmatrix}
=\chi_n(c)
\begin{bmatrix} d_s^n\\ d_{2+s}^n\\ d_{4+s}^n\\ \vdots\\ d_{2r-2+s}^n\\ \vdots\\ d_{2M-4+s}^n\\ d_{2M-2+s}^n \end{bmatrix} \tag{39}$$

The matrix size M, which is larger than $(1/2)[2c/\pi+\log_{10}c]$, is determined such that the resultant eigenvalue and eigenvector in Eq. (39) do not show practical difference as M increases with the relative error 10^{-10}. In addition, the chosen value of M is double-checked by considering the following analytical results as $r=M$ approaches infinity.

$$\text{As } r\to\infty,\qquad A_{2r+s}(c)\to\frac{c^2}{4},\qquad B_{2r+s}(c)\to 4r^2+\frac{c^2}{2}=4M^2+\frac{c^2}{2},\qquad C_{2r+s}(c)\to\frac{c^2}{4} \tag{40}$$

For example, when $c=60$ and $M=40$, Figs. 2a and 2b show some M-component nth eigenvectors of the even- and odd modes, where $n\le[2c/\pi+\log_{10}c]$. Similarly, when $c=600$ and $M=320$, Figs. 3a and 3b show some M-component nth

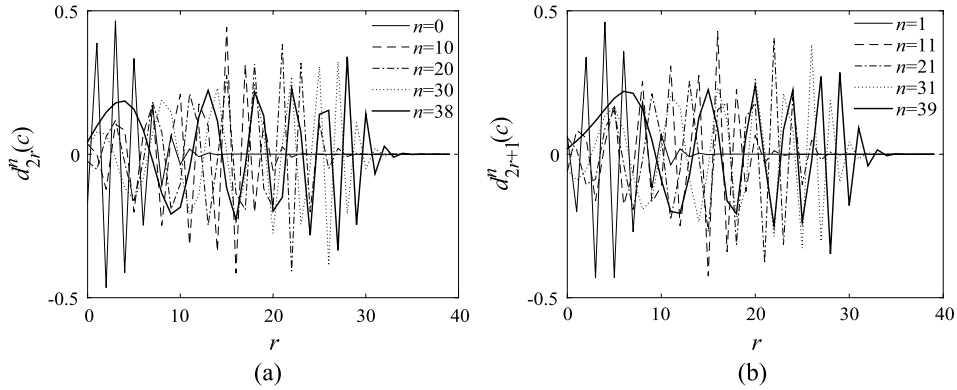

Fig. 2. Some M-component eigenvectors of the even- and odd modes in Eq. (39) when $c = 60$ and $M = 40$. (a) $d^n_{2r}(c)$ ($n = 0, 10, 20, 30, 38$ ($= [2c/\pi + \log_{10} c] - 1$)), (b) $d^n_{2r+1}(c)$; ($n = 1, 11, 21, 31, 39$ ($= [2c/\pi + \log_{10} c]$)), where $r = 0, 1, \ldots, M - 1$.

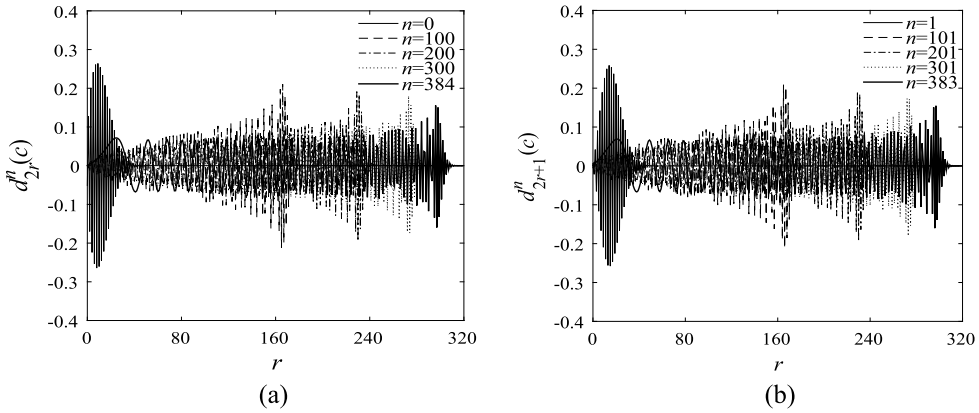

Fig. 3. Some M-component eigenvectors of the even- and odd modes in Eq. (39) when $c = 600$ and $M = 320$. (a) $d^n_{2r}(c)$ ($n = 0, 100, 200, 300, 384$ ($= [2c/\pi + \log_{10} c]$)), (b) $d^n_{2r+1}(c)$ ($n = 1, 101, 201, 301, 383$ ($= [2c/\pi + \log_{10} c] - 1$)), where $r = 0, 1, \ldots, M - 1$.

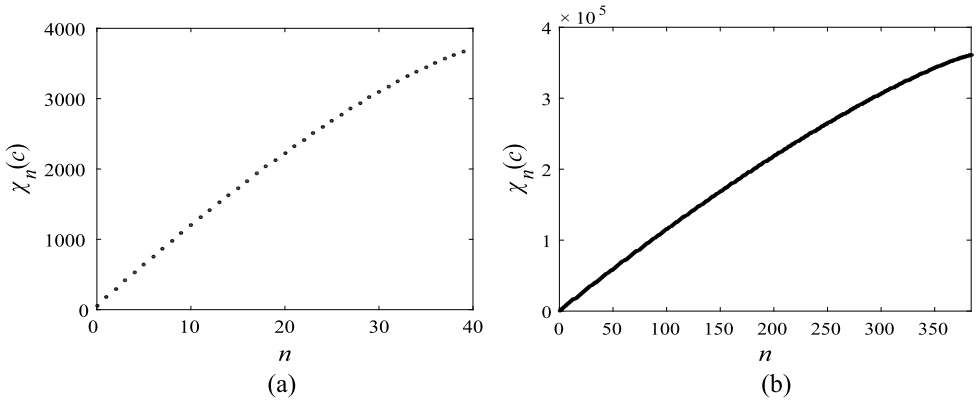

Fig. 4. Eigenvalues $\chi_n(c)$ of PSWF differential equation for (a) $c = 60$ and (b) $c = 600$.

eigenvectors of the even- and odd modes. They are all real. Then, Figs. 4a and 4b show the corresponding eigenvalues $\chi_n(c)$ in Eq. (39) when $c = 60$ and $c = 600$, which are the eigenvalues of the PSWF differential equation. They are all real. Using the values of Fig. 4, Eq. (32) can be calculated, which results in PSWF $S_n(c, \eta)$ for $c = 60$ and $c = 600$ (Figs. 5 and 6). Again, the parameter n is used to denote nth eigenvalues and corresponding eigenvectors in Eq. (39) according to the magnitude of the value of the eigenvalue $\chi_n(c)$ in the increasing order. In addition, even n and odd n correspond to the even and odd functions of PSWFs, respectively (Figs. 5 and 6). The number n also agrees with the number of zero-crossings in each PSWF.

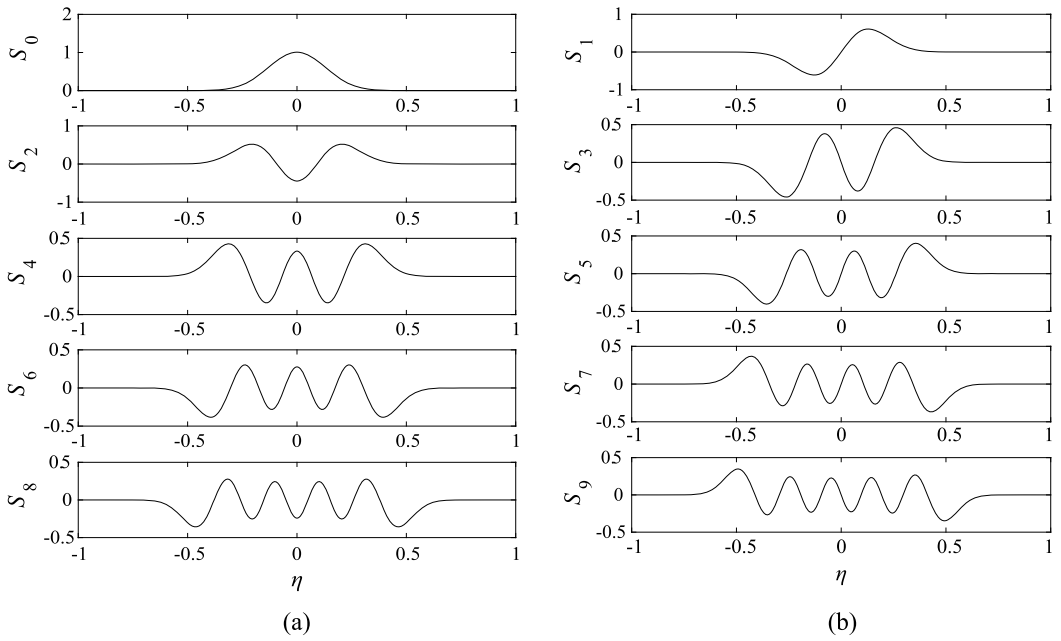

Fig. 5. Prolate spheroidal wave functions $S_n(c, \eta)$ for $c = 60$.

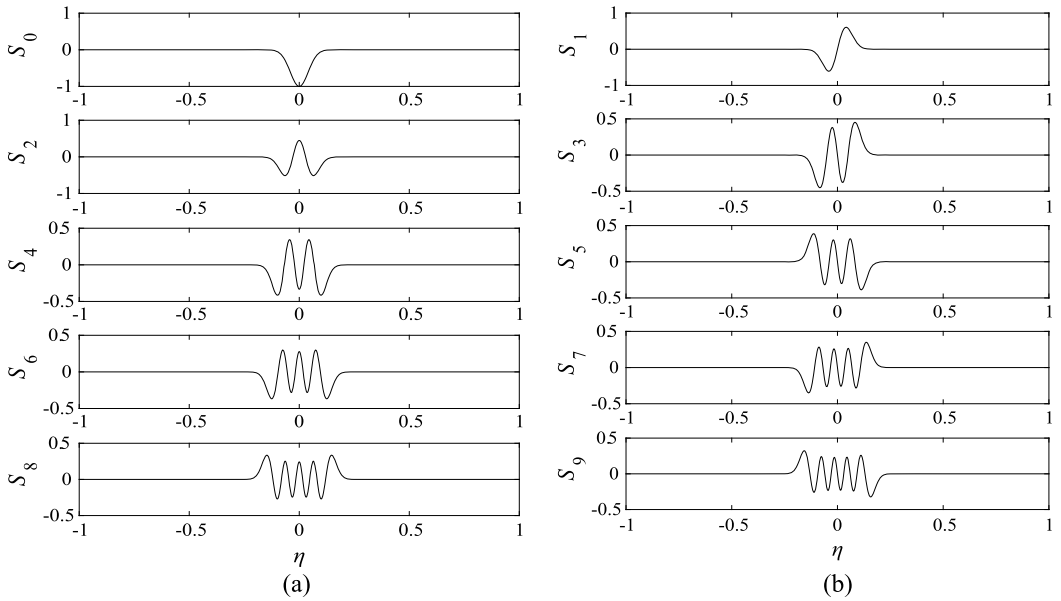

Fig. 6. Prolate spheroidal wave functions $S_n(c, \eta)$ for $c = 600$.

4.2. Eigenvalues of PSWF integral equations

In this subsection, the relationship between eigenvalues $\lambda_n(c)$ of the PSWF integral equation and eigenvalues $\chi_n(c)$ of the PSWF differential equation will be derived.

4.2.1. Even n: $S_n(c, \eta)$ is an even function of η

Let us start from the PSWF integral equation.

$$\int_{-1}^{1} \exp(ic\eta\zeta) S_n(c, \eta) d\eta = \lambda_n(c) S_n(c, \zeta) \tag{41}$$

Then, if $\zeta = 0$,

$$\int_{-1}^{1} S_n(c,\eta)d\eta = \lambda_n(c) S_n(c,0) \tag{42}$$

On the other hand, by integrating the PSWF differential equation from -1 to 1,

$$\int_{-1}^{1} \left(\chi_n(c) - c^2\eta^2\right) S_n(c,\eta)d\eta = 0 \tag{43}$$

or,

$$\int_{-1}^{1} S_n(c,\eta)d\eta = \frac{c^2}{\chi_n(c)} \int_{-1}^{1} \eta^2 S_n(c,\eta)d\eta \tag{44}$$

By equating Eq. (42) and Eq. (44),

$$\lambda_n(c) = \frac{c^2}{\chi_n(c)} \frac{1}{S_n(c,0)} \int_{-1}^{1} \eta^2 S_n(c,\eta)d\eta \tag{45}$$

Then, using the even-ordered Legendre functions,

$$\lambda_n(c) = \frac{c^2}{\chi_n(c)} \frac{1}{S_n(c,0)} \int_{-1}^{1} \eta^2 \sum_{r=0}^{\infty} d_{2r}^n(c) P_{2r}(\eta)d\eta = \frac{c^2}{\chi_n(c)} \frac{1}{S_n(c,0)} \left(\frac{2}{3} d_0^n + \frac{4}{15} d_2^n\right); \quad n = 0, 2, 4, \ldots \tag{46}$$

Therefore, the even-numbered eigenvalues $\lambda_n(c)$; $n = 0, 2, 4, \ldots$ of PSWF integral equation are real.

4.2.2. Odd n: $S_n(c,\eta)$ is an odd function of η

By differentiating PSWF integral equation Eq. (41) with respect to ζ,

$$ic \int_{-1}^{1} \eta \exp(ic\eta\zeta) S_n(c,\eta)d\eta = \lambda_n(c) \frac{dS_n(c,\zeta)}{d\zeta} \tag{47}$$

Then, substitute $\zeta = 0$ into Eq. (47),

$$\int_{-1}^{1} \eta S_n(c,\eta)d\eta = \frac{1}{ic} \lambda_n(c) \left.\frac{dS_n(c,\zeta)}{d\zeta}\right|_{\zeta=0} \tag{48}$$

On the other hand, by multiplying η with PSWF differential equation Eq. (30) and then integrating from -1 to 1 with respect to η,

$$\int_{-1}^{1} \eta \frac{d}{d\eta}\left\{\left(1-\eta^2\right)\frac{dS_n}{d\eta}\right\}d\eta + \int_{-1}^{1} \eta\left(\chi_n(c) - c^2\eta^2\right) S_n(c,\eta)d\eta = 0 \tag{49}$$

The first term in the LHS can be analytically computed by a succession of integrations by parts as follows.

$$\begin{aligned}
&\int_{-1}^{1} \eta \frac{d}{d\eta}\left\{\left(1-\eta^2\right)\frac{dS_n}{d\eta}\right\}d\eta = \int_{-1}^{1} \eta\left(1-\eta^2\right)\frac{d^2S_n}{d\eta^2}d\eta - \int_{-1}^{1} 2\eta^2 \frac{dS_n}{d\eta}d\eta \\
&= \left[\eta\left(1-\eta^2\right)\frac{dS_n}{d\eta}\right]_{-1}^{1} - \int_{-1}^{1} \left(1-3\eta^2\right)\frac{dS_n}{d\eta}d\eta - \left[2\eta^2 S_n(c,\eta)\right]_{-1}^{1} + \int_{-1}^{1} 4\eta S_n(c,\eta)d\eta \\
&= -\left[\left(1-3\eta^2\right)S_n(c,\eta)\right]_{-1}^{1} + \int_{-1}^{1} (-6\eta) S_n(c,\eta)d\eta - \left[2\eta^2 S_n(c,\eta)\right]_{-1}^{1} + \int_{-1}^{1} 4\eta S_n(c,\eta)d\eta
\end{aligned}$$

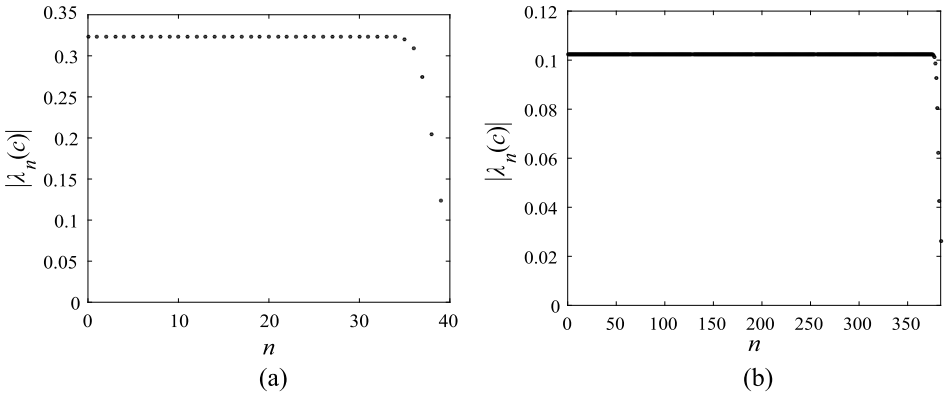

Fig. 7. Absolute value of eigenvalues $|\lambda_n(c)|$ of PSWF integral equation for (a) $c = 60$, (b) $c = 600$.

$$= 2S_n(c,1) - 2S_n(c,-1) - 2S_n(c,1) + 2S_n(c,-1) - 2\int_{-1}^{1} \eta S_n(c,\eta)d\eta = -2\int_{-1}^{1} \eta S_n(c,\eta)d\eta \tag{50}$$

Thus, by substituting Eq. (50) into Eq. (49),

$$\int_{-1}^{1} \eta S_n(c,\eta)d\eta = \frac{c^2}{\chi_n(c) - 2}\int_{-1}^{1} \eta^3 S_n(c,\eta)d\eta \tag{51}$$

Now, by comparison of Eq. (51) with Eq. (48),

$$\lambda_n(c) = \frac{ic^3}{\chi_n(c) - 2}\frac{1}{dS_n/d\zeta\,|_{\zeta=0}}\int_{-1}^{1} \eta^3 S_n(c,\eta)d\eta \tag{52}$$

Then, using the odd-numbered Legendre functions,

$$\begin{aligned}\lambda_n(c) &= \frac{ic^3}{\chi_n(c) - 2}\frac{1}{dS_n/d\zeta\,|_{\zeta=0}}\int_{-1}^{1} \eta^3 \sum_{r=0}^{\infty} d_{2r+1}^n(c) P_{2r+1}(\eta)d\eta \\ &= \frac{ic^3}{\chi_n(c) - 2}\frac{1}{dS_n/d\zeta\,|_{\zeta=0}}\left(\frac{2}{5}d_1^n + \frac{4}{35}d_3^n\right); \quad n = 1,3,5,\ldots\end{aligned} \tag{53}$$

Therefore, the odd-numbered eigenvalues $\lambda_n(c)$; $n = 1,3,5,\ldots$ of PSWF integral equation are purely imaginary. Figs. 7a and 7b show the absolute values of eigenvalues of PSWF integral equation for $c = 60$ and $c = 600$, respectively, which are derived from eigenvalues $\chi_n(c)$ of PSWF differential equation and PSWF $S_n(c,\eta)$. As shown, as the numbering increases from $n = 0$, the eigenvalues remains constant and, about at $[2c/\pi + \log_{10} c]$, the eigenvalues thereafter drop to zeros.

5. Semi-analytical Karhunen–Loeve representation of random data based on PSWF

In this section, based on the results in the previous sections, we will suggest a semi-analytical K–L representation of time-limited ($-T \le t \le T$) and band-limited ($-\Omega \le \omega \le \Omega$) random data $\zeta_N(t)$ based on PSWF. The dimensionless parameter $c = \Omega T$.

$$\zeta_N(t) = \sum_{j=0}^{N-1} a_j\phi_j(t); \qquad a_j = \int_{-T}^{T} \zeta(t)\phi_j(t)dt, \qquad \int_{-T}^{T} \phi_i(t)\phi_j(t)dt = \delta_{ij}, \tag{54}$$

where the basis $\phi_j(t)$ satisfies the following integral equation.

$$\int_{-T}^{T} K(t-t')\phi_j(t')dt' = \kappa_j\phi_j(t) \tag{55}$$

The integral equation Eq. (55) is equivalent to the following matrix eigenvalue problem [14] and the detailed derivation is given in Appendix A.

$$\left[c\lambda_j(c)\lambda_k(c)G_{jk}\right]A_k^i = \kappa_i A_j^i, \tag{56}$$

$$G_{jk} = \frac{1}{2\pi}\int_{-\Omega}^{\Omega} P(\omega)S_j\left(c,\frac{\omega}{\Omega}\right)S_k\left(c,\frac{\omega}{\Omega}\right)\frac{1}{\Omega}d\omega \tag{57}$$

where S_j denotes the PSWF. In the above, $\lambda_j(c)$ is the eigenvalue of the PSWF integral equation.

The detailed solution procedure is summarized as follows.

Step 1) For a chosen c, find PSWF $S_n(c,\eta)$ and $\chi_n(c)$ derived from the PSWF differential equation

$$\frac{d}{d\eta}\left\{(1-\eta^2)\frac{dS_n(c,\eta)}{d\eta}\right\} + \left(\chi_n(c) - c^2\eta^2\right)S_n(c,\eta) = 0 \tag{30}$$

$$S_n(c,\eta) = \sum_{r=0}^{M-1} d_{2r+s}^n(c)P_{2r+s}(\eta); \quad s = \begin{cases} 0 & (n=0,2,4,\ldots) \\ 1 & (n=1,3,5,\ldots), \end{cases} \tag{32}$$

$$A_{2r+s}d_{2r-2+s}^n + B_{2r+s}d_{2r+s}^n + C_{2r+s}d_{2r+2+s}^n = \chi_n(c)d_{2r+s}^n; \quad r=0,1,2,\ldots,M-1, \ (M \text{ by } M) \tag{33}$$

Step 2) Find $\lambda_n(c)$ from the solutions in Eqs. (32) and (33) above, derived from the relationship between PSWF differential equation Eq. (30) and integral equation Eq. (29).

$$\int_{-1}^{1} S_n \exp(ic\eta\zeta)d\eta = \lambda_n(c)S_n \tag{29}$$

$$\lambda_n(c) = \frac{c^2}{\chi_n(c)}\frac{1}{S_n(c,0)}\left(\frac{2}{3}d_0^n + \frac{4}{15}d_2^n\right); \quad n=0,2,4,\ldots \tag{46}$$

$$\lambda_n(c) = \frac{ic^3}{\chi_n(c)-2}\frac{1}{dS_n/d\zeta|_{\zeta=0}}\left(\frac{2}{5}d_1^n + \frac{4}{35}d_3^n\right); \quad n=1,3,5,\ldots \tag{53}$$

Step 3) Solve the following eigenvalue problem derived from the relationship between PSWF integral equation Eq. (29) and K–L expansion Eq. (55), using Eqs. (32), (46) and (53).

$$\int_{-T}^{T} K(t-t')\phi_j(t')dt' = \kappa_j\phi_j(t), \tag{55}$$

$$\left[c\lambda_j(c)\lambda_k(c)G_{jk}\right]A_k^i = \kappa_i A_j^i, \quad \left(M' \text{ by } M';\ M' = [2c/\pi + \log_{10}c] + 1\right) \tag{56}$$

$$G_{jk} = \frac{1}{2\pi}\int_{-\Omega}^{\Omega} P(\omega)S_j\left(c,\frac{\omega}{\Omega}\right)S_k\left(c,\frac{\omega}{\Omega}\right)\frac{1}{\Omega}d\omega, \tag{57}$$

Step 4) Find bases $\phi_i(t)$ using Eqs. (32) and (56)

$$\phi_i(t) = \sum_{j=0}^{M-1} A_j^i S_j\left(c,\frac{t}{T}\right) \tag{A.13}$$

Step 5) Represent N-point data $\zeta_N(t)$ using bases found in Eq. (A.13).

$$a_j = \int_{-T}^{T} \zeta_N(t)\phi_j(t)dt; \quad j=0,1,2,\ldots,[2c/\pi + \log c] \tag{54}$$

- Single basis representation: $\zeta_N^{(1)}(t) = a_0\phi_0(t)$
- Two-basis representation: $\zeta_N^{(2)}(t) = \sum_{j=0}^{1} a_j\phi_j(t)$
- M'-basis representation: $\zeta_N^{(M')}(t) = \sum_{j=0}^{M'-1} a_j\phi_j(t)$

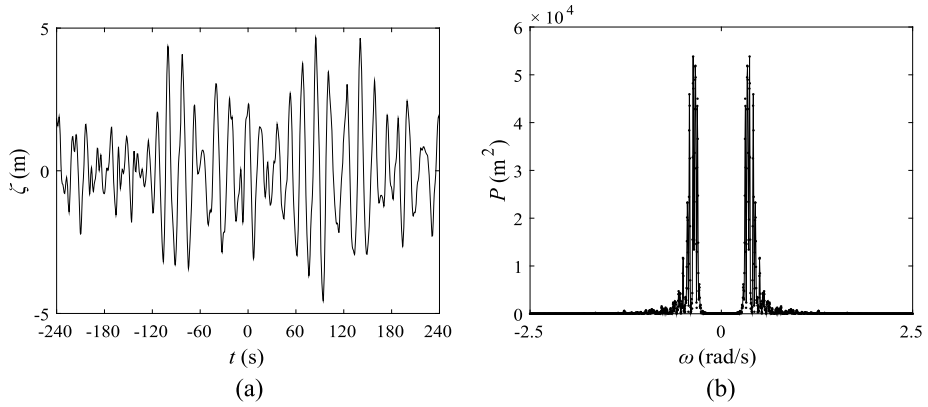

Fig. 8. Wave elevation data (a) temporal data $\zeta(t)$, (b) spectral data $P(\omega)$.

Table 1
Information on the wave data.

Name	Harvest, CA
Station	07101
Deployment latitude	34.27.340′N
Deployment longitude	120.47.000′W
Water depth	548.64 m
Sample rate	3.48 Hz
Start time	February 24, 2008, 21:04 UTC
End time	February 24, 2008, 21:34 UTC
Sample length	30 minutes
Significant height	9.97 m
Maximum height	20.59 m

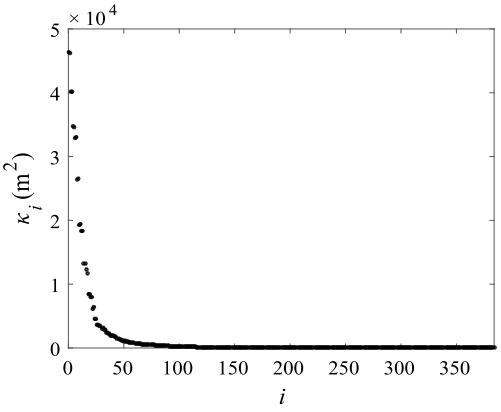

Fig. 9. Eigenvalues of $[c\lambda_j(c)\lambda_k(c)G_{jk}]$ in (67); $i = 0, 1, \ldots, 384$ $(= [2c/\pi + \log c])$.

5.1. Example: ordinary irregular waves

Figs. 8a and 8b show the temporal- and spectral wave elevation data from the thirty-minute buoy measurement data (US west coast) of CDIP (Coastal Data Information Program) webpage (https://cdip.ucsd.edu/) [19]. The number of data points are $N = 1845$. The overall information of data is summarized in Table 1. Here, the selected real measure times are eight minutes (21:23–21:31). The purpose here is to analyze or to decompose the temporal data $\zeta_N(t)$ (Fig. 8a) using the K–L representation based on the spectral data $P(\omega)$ (Fig. 8b) from the temporal data themselves, PSWF, eigenvalues of PSWF differential equations $\chi_n(c)$ or, equivalently eigenvalues of PSWF integral equations $\lambda_n(c)$, and the relevant parameters $T = 240$ (s), $\Omega = 2.5$ (rad/s), $c = \Omega T = 600$. In the computation of Eq. (39), i.e. PSWF and $\chi_n(c)$, the matrix size for the even and odd case each is set to be M by M ($M = 320$) which is much smaller than N by N ($N = 1845$), where M is chosen such that $[2c/\pi + \log_{10} c]/2 < M << N$. For $c = 600$, the numbers of eigenvalues and eigenvectors (PSWFs) are total 385 ($n = 0$ to $n = [2c/\pi + \log_{10} c] = 384$); 193 for the even modes and 192 for the odd modes. For each even and odd case, using these 193 and 192 PSWFs and $\chi_n(c)$s, respectively, we solve 193 by 193 and 192 by 192 matrix eigenvalue problem Eqs. (56) and (57) numerically and, as a result, 385 eigenvalues κ_i (Fig. 9) and the associated 385 eigenvectors A_j^i are

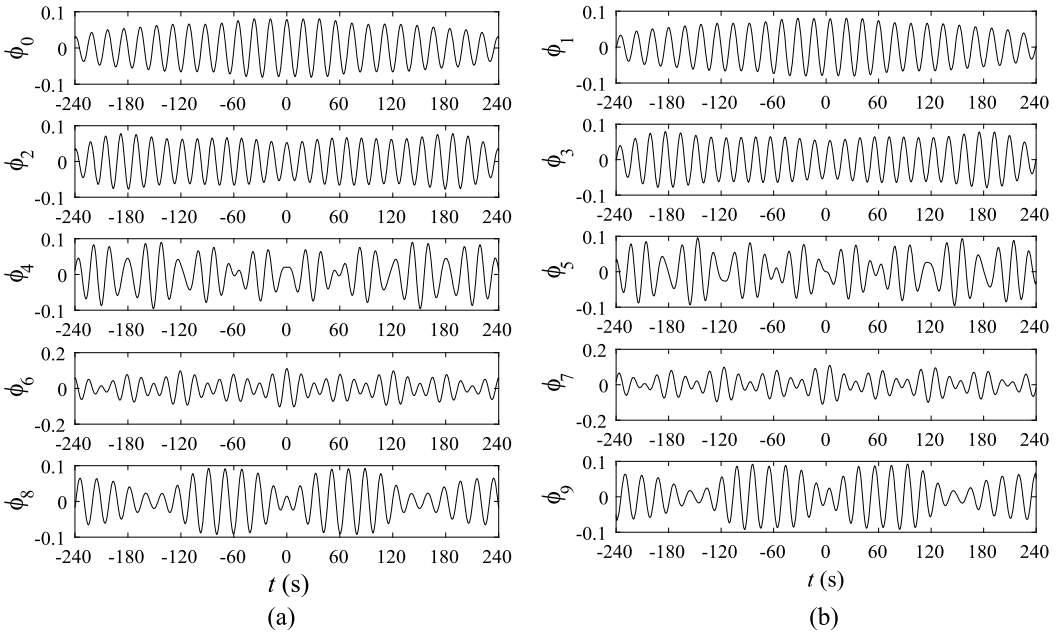

Fig. 10. Base functions $\phi_j(t)$; $j = 0, 1, 2, \ldots, 9$.

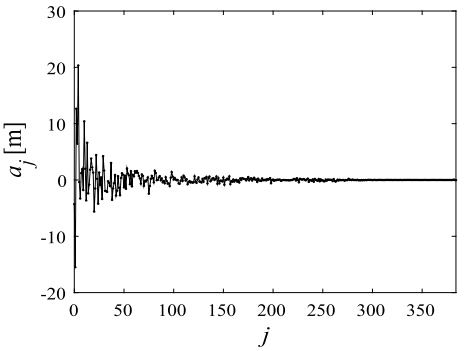

Fig. 11. Coefficients $a_j = \int_{-T}^{T} \zeta(t)\phi_j(t)dt$; $j = 0, 1, \ldots, 384$ $(= [2c/\pi + \log_{10} c])$.

obtained accurately and easily, thanks to its small size. Then, using those 385 eigenvectors and 385 PSWFs $S_j(c, t/T)$, from Eq. (A.13), 385 bases $\phi_i(t)$ are obtained (Fig. 10). Now, from Eq. (54), $a_j = \int_{-T}^{T} \zeta_N(t)\phi_j(t)dt$ ($j = 0$ to 384) can be calculated and ordered according to its absolute value as shown in Fig. 11. Finally, the temporal wave-elevation data $\zeta_N(t)$ can be fully but approximately reconstructed by $\zeta_N(t) \approx \zeta_{N=1845}^{(385)}(t) \approx \sum_{j=0}^{384} a_j\phi_j(t)$. In Fig. 12, we show partial sums $\zeta_{1845}^{(25)}(t)$, $\zeta_{1845}^{(50)}(t)$, $\zeta_{1845}^{(150)}(t)$, $\zeta_{1845}^{(385)}(t)$, where the subscript denotes the number of data points and the superscript the number of bases used.

Finally, according to the number of bases used, the semi-analytical K–L expansion using PSWF is compared with the direct numerical K–L expansion and a semi-analytical K–L expansion using sinusoidal functions, in terms of its closeness to the original data (norm) as shown in Fig. 13. Both results of the direct numerical K–L expansion and a semi-analytical K–L representation using sinusoidal functions perfectly agree with the present semi-analytical K–L expansion result (graphically perfectly overlapped in Fig. 13). The difference between them is the computational efficiency. First, for the direct numerical calculation of K–L expansion, we need to solve Eqs. (1), (2) and (3) using a bigger matrix (1845 by 1845). In Appendix B, the discretization of Eq. (1) for the direct calculation of K–L expansion is described. For this particular example, with the same accuracy, the computation time of the direct numerical K–L expansion (10.6 s) is shorter than the PSWF-based semi-analytical method (19.2 s), which is measured using the command “etime” in Matlab. The overall comparison is summarized in Table 2. For the semi-analytical K–L representation using sinusoidal functions, the overall procedure of the present semi-analytical method using the PSWF (Appendix A) is modified such that following sinusoidal functions are used as bases instead of the PSWF

$$\left\{1, \cos\frac{\pi}{2T}t, \sin\frac{\pi}{2T}t, \ldots, \cos\frac{n\pi}{2T}t, \sin\frac{n\pi}{2T}t, \ldots\right\}, \tag{58}$$

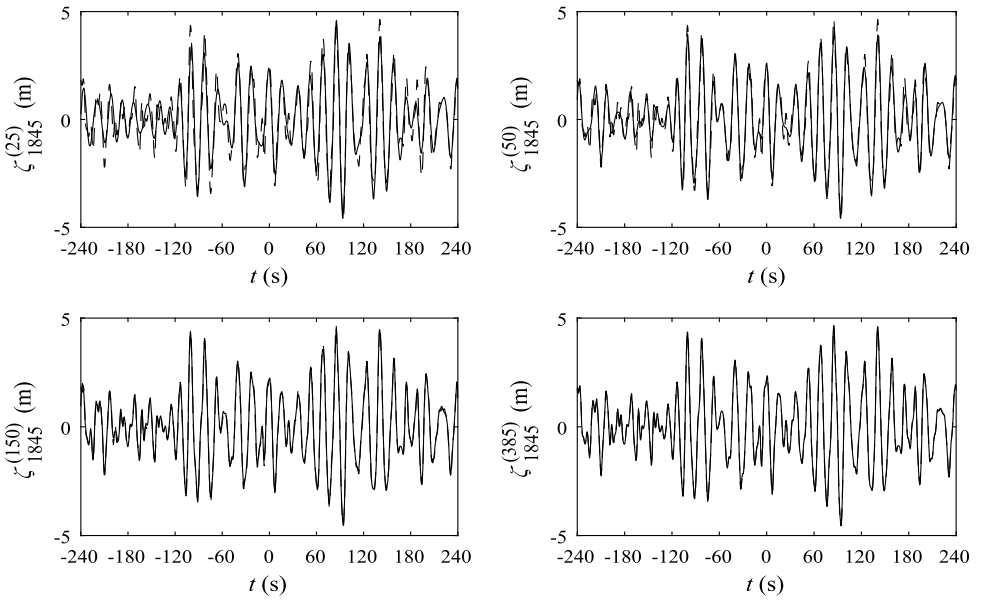

Fig. 12. Reconstruction of the original wave-elevation data $\zeta^{(M')}_{N=1845}(t)$, where the subscript denotes the number of data points and the superscript the number of bases used. The dashed line is the original wave-elevation data, the solid line is the reconstructed data. (a) $M' = 25$, (b) $M' = 50$, (c) $M' = 150$, (d) $M' = 385 = [2c/\pi + \log_{10} c] + 1$.

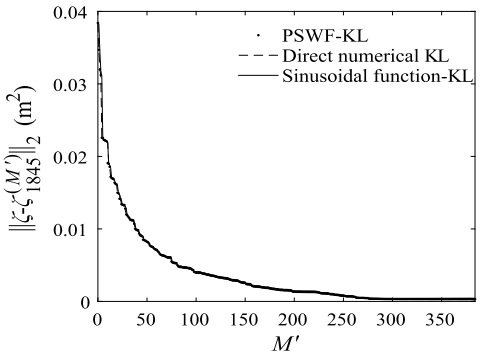

Fig. 13. Error between the original wave-elevation data and the reconstructed data. The dotted line is the error in K–L representation based on PSWF (PSWF-KL), the dashed line is the error in direct numerical K–L representation, and the solid line is the error in K–L representation based on sinusoidal functions.

Table 2
Computational efficiency. (a) Semi-analytical K–L expansion using PSWF, (b) Direct numerical K–L expansion, (c) Semi-analytical K–L expansion using sinusoidal functions.

Computational methods	Equations	Matrix size	Computation time (s)
(a) Semi-analytical K–L expansion using PSWF	Eq. (33): even mode	320 by 320	19.2
	Eq. (33): odd mode	320 by 320	
	Eq. (56): even mode	193 by 193	
	Eq. (56): odd mode	192 by 192	
(b) Direct numerical K–L expansion	Eq. (55)	1845 by 1845	10.6
(c) Semi-analytical K–L expansion using sinusoidal functions	Eq. (59): even mode	400 by 400	122.5
	Eq. (60): odd mode	400 by 400	

which is used in Mulani et al. [15]. Then, after the similar derivation to the PSWF case, the resultant matrix eigenvalue problems will be, for the even and the odd modes, respectively,

$$\kappa_j d_{nj} = \sum_{m=0}^{M'_S-1} d_{mj} P\left(\omega = \frac{n\pi}{2T}\right) \int_{-T}^{T} \cos\left(\frac{n\pi}{2T}t'\right) \cos\left(\frac{m\pi}{2T}t'\right) dt', \tag{59}$$

$$\kappa_j d_{nj} = \sum_{m=0}^{M_S'-1} d_{mj} P\left(\omega = \frac{n\pi}{2T}\right) \int_{-T}^{T} \sin\left(\frac{n\pi}{2T}t'\right) \sin\left(\frac{m\pi}{2T}t'\right) dt' \tag{60}$$

For the same exemplary data ($N = 1845$), the matrix size for the even and odd case each is set to be 400 by 400 by trial and error. With the same accuracy, the computation time of the semi-analytical method using sinusoidal functions (122.5 s) is much longer than the PSWF-based semi-analytical method (19.2 s) as shown in Table 2.

6. Concluding remark

The method suggested in this work would be a useful alternative to the conventional direct numerical K–L representation for moderate-size data. The direct numerical approach may suffer from the computational inaccuracy for big data. In this case, the present method will successfully provide relatively small but necessary number of bases for the accurate representation of the given data. The present method can be used to analyze many kinds of random data in fluid mechanics (e.g., waves, turbulent flows) and, in particular, will be useful for big wave data and turbulent-flow data.

Acknowledgements

This work was supported by the National Research Foundation of Korea (NRF) (2017R1D1A1B03028299).

Appendix A. Formulation of the matrix eigenvalue problem for the basis ϕ_j

According to Karhunen–Loeve theorem, a basis function $\phi_j(t)$ which minimizes the mean squared error between the original data and the truncated version of it will satisfy following integral equation.

$$\int_{-T}^{T} K(t-t')\phi_j(t')dt' = \kappa_j \phi_j(t), \tag{A.1}$$

where

$$K(t-t') = \frac{1}{2T}\int_{-T}^{T} \zeta(t)\zeta(t-t')dt = \frac{1}{2\pi}\int_{-\infty}^{\infty} P(\omega)\exp\big(i\omega(t-t')\big)d\omega \tag{A.2}$$

Now, according to Mercer's theorem, since the kernel $K(t-t')$ is both symmetric and positive definite, this can be represented with the orthonormal eigenfunctions and the eigenvalues as follows.

$$K(t-t') = \sum_{j=0}^{\infty} \kappa_j \phi_j(t)\phi_j(t') \tag{A.3}$$

For the purpose of analysis, we define following dimensionless parameters.

$$\frac{\omega}{\Omega} \equiv \omega', \qquad \frac{t}{T} \equiv \tau', \qquad \Omega T \equiv c \tag{A.4}$$

Then, the PSWS integral equation is

$$\int_{-1}^{1} \exp\big(ic\omega'\tau'\big) S_j(c,\omega')d\omega' = \lambda_j(c) S_j(c,\tau') \tag{A.5}$$

where the exponential term

$$\exp\big(ic\omega'\tau'\big) = \exp\left(iT\Omega\frac{\omega}{\Omega}\frac{t}{T}\right) = \exp(i\omega t). \tag{A.6}$$

Using Mercer's theorem,

$$\exp(i\omega t) = \exp\big(ic\omega'\tau'\big) = \sum_{j=0}^{\infty} \lambda_j(c) S_j(c,\omega') S_j(c,\tau') \tag{A.7}$$

Then, from Eqs. (A.2) and (A.7),

$$
\begin{aligned}
K(t-t') &= \frac{1}{2\pi}\int_{-\infty}^{\infty} P(\omega)\exp(-i\omega t')\exp(i\omega t)d\omega \\
&= \frac{1}{2\pi}\int_{-\infty}^{\infty} P(\omega)\exp(-i\omega t')\left\{\sum_{j=0}^{\infty}\lambda_j(c)S_j(c,\omega')S_j(c,\tau')\right\}d\omega \\
&= \sum_{j=0}^{\infty}\left[\lambda_j(c)S_j(c,\tau')\left\{\frac{1}{2\pi}\int_{-\infty}^{\infty} P(\omega)\exp(-i\omega t')S_j(c,\omega')d\omega\right\}\right] \\
&\equiv \sum_{j=0}^{\infty}\lambda_j(c)S_j(c,\tau')\Psi_j(t'),
\end{aligned}
\tag{A.8}
$$

where

$$
\Psi_j(t') = \frac{1}{2\pi}\int_{-\infty}^{\infty} P(\omega)\exp(-i\omega t')S_j\left(c,\frac{\omega}{\Omega}\right)d\omega \tag{A.9}
$$

Then, by comparison with Eq. (A.3),

$$
\sum_{i=0}^{\infty}\kappa_i\phi_i(t)\phi_i(t') = \sum_{j=0}^{\infty}\lambda_j(c)S_j\left(c,\frac{t}{T}\right)\Psi_j(t') \tag{A.10}
$$

By performing $\int_{-T}^{T}\phi_k(t')\times$ Eq. (A.10)dt',

$$
\sum_{i=0}^{\infty}\kappa_i\phi_i(t)\int_{-T}^{T}\phi_i(t')\phi_k(t')dt' = \sum_{j=0}^{\infty}\lambda_j(c)S_j\left(c,\frac{t}{T}\right)\int_{-T}^{T}\Psi_j(t')\phi_k(t')dt' \tag{A.11}
$$

Using the orthonormal property $\int_{-T}^{T}\phi_i(t)\phi_j(t)dt = \delta_{ij}$,

$$
\kappa_i\phi_i(t) = \sum_{j=0}^{\infty}\lambda_j(c)S_j\left(c,\frac{t}{T}\right)\int_{-T}^{T}\Psi_j(t')\phi_k(t')dt' \tag{A.12}
$$

or

$$
\phi_i(t) = \sum_{j=0}^{\infty}\left\{\frac{\lambda_j(c)}{\kappa_i}\int_{-T}^{T}\Psi_j(t')\phi_k(t')dt'\right\}S_j\left(c,\frac{t}{T}\right) \equiv \sum_{j=0}^{\infty}A_j^iS_j\left(c,\frac{t}{T}\right) \tag{A.13}
$$

This is the implicit equation for ϕ_i. To eliminate ϕ_i, from Eqs. (A.12) and (A.13),

$$
\sum_{j=0}^{\infty}(\kappa_iA_j^i)S_j\left(c,\frac{t}{T}\right) = \sum_{j=0}^{\infty}\left\{\sum_{k=0}^{\infty}A_k^i\lambda_j(c)\left\{\int_{-T}^{T}\Psi_j(t')S_k\left(c,\frac{t'}{T}\right)dt'\right\}\right\}S_j\left(c,\frac{t}{T}\right) \tag{A.14}
$$

Then, by comparing the coefficient of $S_j(c,\frac{t}{T})$ in both sides,

$$
\kappa_iA_j^i = \sum_{k=0}^{\infty}A_k^i\lambda_j(c)\left\{\int_{-T}^{T}\Psi_j(t')S_k\left(c,\frac{t'}{T}\right)dt'\right\} \equiv \sum_{k=0}^{\infty}A_k^i\lambda_j(c)D_{kj} \tag{A.15}
$$

Using Eq. (A.9),

$$
\begin{aligned}
D_{kj} &= \int_{-T}^{T}\left\{\frac{1}{2\pi}\int_{-\infty}^{\infty}P(\omega)\exp(-i\omega t')S_j\left(c,\frac{\omega}{\Omega}\right)d\omega\right\}S_k\left(c,\frac{t'}{T}\right)dt' \\
&= \frac{1}{2\pi}\int_{-\infty}^{\infty}P(\omega)S_j\left(c,\frac{\omega}{\Omega}\right)\left\{\int_{-T}^{T}\exp(-i\omega t')S_k\left(c,\frac{t'}{T}\right)dt'\right\}d\omega
\end{aligned}
\tag{A.16}
$$

By letting $t'/T = u$ and using $\omega/\Omega = \omega'$ and $c = \Omega T$,

$$\int_{-T}^{T} \exp(-i\omega t') S_k\left(c, \frac{t'}{T}\right) dt' = T \int_{-1}^{1} \exp(-i\Omega\omega' uT) S_k(c,u) du = T \int_{-1}^{1} \exp(-ic\omega' u) S_k(c,u) du \tag{A.17}$$

Using $T\int_{-1}^{1} \exp(-ic\omega' u) S_k(c,u) du = T\int_{-1}^{1} \exp(ic\omega' u) S_k(c,u) du = T\lambda_k(c) S_k(c,\omega')$ Eq. (A.5), it follows that

$$\begin{aligned} D_{kj} &= \frac{1}{2\pi} \int_{-\infty}^{\infty} P(\omega) S_j\left(c, \frac{\omega}{\Omega}\right) T\lambda_k(c) S_k(c,\omega') d\omega \\ &= (T\Omega)\lambda_k(c) \frac{1}{2\pi} \int_{-\infty}^{\infty} P(\omega) S_j\left(c, \frac{\omega}{\Omega}\right) S_k\left(c, \frac{\omega}{\Omega}\right) d\left(\frac{\omega}{\Omega}\right) \equiv c\lambda_k(c) G_{jk} \end{aligned} \tag{A.18}$$

Then, from Eqs. (A.15) and (A.18),

$$\kappa_i A_j^i = \sum_{k=0}^{\infty} c\lambda_j(c)\lambda_k(c) G_{jk} A_k^i \equiv \left[c\lambda_j(c)\lambda_k(c) G_{jk}\right] A_k^i \tag{A.19}$$

Appendix B. Discretization of Eq. (1) for the direct numerical K–L expansion

$$\int_{-T}^{T} K(t-t')\phi_j(t) dt = \kappa_j \phi_j(t'), \tag{B.1}$$

As a first step for the discretization of Eq. (B.1), the time is discretized as follows.

$$t_n, t_n' = -T + n\Delta t; \qquad \Delta t = \frac{2T}{N-1}, \quad n = 0, 1, \ldots, N-1 \tag{B.2}$$

Then, at time $t_n' = -T$, from Eq. (B.1),

$$\int_{-T}^{T} K(t-(-T))\phi_j(t) dt \approx \sum_{n=0}^{N-1} K(t_n + T)\phi_j(t_n) = \sum_{n=0}^{N-1} K(n\Delta t)\phi_j(-T + n\Delta t) = \kappa_j \phi_j(-T) \tag{B.3}$$

or, in matrix form,

$$\left[K(0), K(\Delta t), K(2\Delta t), \ldots, K(2T)\right]\left[\phi_j(-T), \phi_j(-T+\Delta t), \phi_j(-T+2\Delta t), \ldots, \phi_j(T)\right]^T = \kappa_j \phi_j(-T) \tag{B.4}$$

Similarly, at time $t_n' = -T + \Delta t$,

$$\begin{aligned} &\left[K(-\Delta t), K(0), K(\Delta t), \ldots, K(2T-\Delta t)\right]\left[\phi_j(-T), \phi_j(-T+\Delta t), \phi_j(-T+2\Delta t), \ldots, \phi_j(T)\right]^T \\ &= \kappa_j \phi_j(-T+\Delta t) \end{aligned} \tag{B.5}$$

This way, Eq. (B.1) can be discretized as follows.

$$\begin{bmatrix} K(0) & K(\Delta t) & K(2\Delta t) & \cdots & K(2T) \\ K(-\Delta t) & K(0) & K(\Delta t) & \cdots & K(2T-\Delta t) \\ K(-2\Delta t) & K(-\Delta t) & K(0) & \cdots & K(2T-2\Delta t) \\ \vdots & \vdots & \vdots & \ddots & \vdots \\ K(-2T) & K(-2T+\Delta t) & K(-2T+2\Delta t) & \cdots & K(0) \end{bmatrix} \begin{bmatrix} \phi_j(-T) \\ \phi_j(-T+\Delta t) \\ \phi_j(-T+2\Delta t) \\ \vdots \\ \phi_j(T) \end{bmatrix} = \kappa_j \begin{bmatrix} \phi_j(-T) \\ \phi_j(-T+\Delta t) \\ \phi_j(-T+2\Delta t) \\ \vdots \\ \phi_j(T) \end{bmatrix} \tag{B.6}$$

References

[1] H.P. Bakewell Jr., J.L. Lumley, Viscous sublayer and adjacent wall region in turbulent pipe flow, Phys. Fluids 10 (1967) 1880–1889, http://dx.doi.org/10.1063/1.1762382.
[2] D. Chambers, R. Adrian, P. Moin, D. Stewart, H. Sung, Karhunen–Loeve expansion of Burgers model of turbulence, Phys. Fluids 31 (1988) 2573–2582, http://dx.doi.org/10.1063/1.866535.
[3] P. Moin, R.D. Moser, Characteristic eddy decomposition of turbulence in a channel, J. Fluid Mech. 200 (1989) 471–509, http://doi.org/10.1017/S0022112089000741.

[4] G.A. Webber, R.A. Handler, L. Sirovich, The Karhunen–Loeve decomposition of minimal channel flow, Phys. Fluids 9 (1997) 1054–1066, http://dx.doi.org/10.1063/1.869323.
[5] B.R. Noack, K. Afanasiev, M. Morzynski, G. Tanmor, F. Thiele, A hierarchy of low-dimensional models for the transient and post-transient cylinder wake, J. Fluid Mech. 497 (2003) 335–363, http://doi.org/10.1017/S0022112003006694.
[6] K.S. Breuer, L. Sirovich, The use of the Karhunen–Loeve procedure for the calculation of linear eigenfunctions, J. Comput. Phys. (1991) 277–296, http://dx.doi.org/10.1016/0021-9991(91)90237-F.
[7] K. Hasselmann, T.P. Barnett, E. Bouws, H. Carlson, D.E. Cartwright, K. Enke, J.A. Ewing, H. Gienapp, D.E. Hasselmann, P. Kruseman, A. Meerbug, P. Muller, D.J. Olbers, K. Richter, W. Sell, H. Walden, Measurements of Wind-Wave Growth and Swell Decay During the Joint North Sea Wave Project (JONSWAP), Deutches Hydrographisches Institut, Hamburg, 1973, uuid:f204e188-13b9-49d8-a6dc-4fb7c20562fc.
[8] W.J. Pierson, L. Moskowitz, A proposed spectral form for fully developed wind sea based on the similarity theory of S.A. Kitaigorodskii, J. Geophys. Res. 69 (1964) 5181–5190, http://dx.doi.org/10.1029/JZ069i024p05181.
[9] J. Mercer, Functions of positive and negative type, and their connection with the theory of integral equations, Philos. Trans. R. Soc. A. 209 (1909) 415–446, http://doi.org/10.1098/rsta.1909.0016.
[10] C. Flammer, Spheroidal Wave Functions, Stanford University Press, 1957.
[11] D. Slepian, H.O. Pollak, Prolate spheroidal wave functions, Fourier analysis and uncertainty I, Bell Labs Tech. J. 40 (1961) 43–63, http://doi.org/10.1002/j.1538-7305.1961.tb03976.x.
[12] J. Mathews, R.L. Walker, Mathematical Methods of Physics, W. A. Benjamin, New York, 1970.
[13] A. Osipov, Certain inequalities involving prolate spheroidal wave functions and associated quantities, Appl. Comput. Harmon. Anal. 35 (2013) 359–393, http://dx.doi.org/10.1016/j.acha.2012.10.002.
[14] P.D. Sclavounos, Karhunen–Loeve representation of stochastic ocean waves, Proc. R. Soc. A 468 (2012) 2574–2594, http://doi.org/10.1098/rspa.2012.0063.
[15] S.B. Mulani, R.K. Kapania, K.M. Scott, Generalized linear random vibration analysis using autocovariance orthogonal decomposition, AIAA J. 48 (8) (2010) 1652–1661, http://dx.doi.org/10.2514/1.J050033.
[16] S.P. Huang, S.T. Quek, K.K. Phoon, Convergence study of the truncated Karhunen–Loeve expansion for simulation of stochastic processes, Int. J. Numer. Methods Eng. 52 (9) (2001) 1029–1043, http://dx.doi.org/10.1002/nme.255.
[17] K.K. Phoon, S.P. Huang, S.T. Quek, Implementation of Karhunen–Loeve expansion for simulation using a wavelet-Galerkin scheme, Probab. Eng. Mech. 17 (3) (2002) 293–303, http://dx.doi.org/10.1016/S0266-8920(02)00013-9.
[18] Y. Ikebe, N. Asai, Y. Miyazaki, D. Cai, The eigenvalue problem for infinite complex symmetric tridiagonal matrices with application, Linear Algebra Appl. 241 (1996) 599–618, http://dx.doi.org/10.1016/0024-3795(95)00699-0.
[19] Scripps Institution of Oceanography, The Coastal Data Information Program (CDIP), https://cdip.ucsd.edu/?nav=historic&sub=data&units=metric&tz=UTC&pub=public&map_stati=1,2,3&stn=071&stream=p1.